IUST Iran University of Science and Technology

Iranian Journal of Electrical and Electronic Engineering

Journal Homepage: ijeee.iust.ac.ir

Research Paper

Analytical Field Study on Induction Motors under Fluctuated Voltages

M. Ghaseminezhad*(C.A.), A. Doroudi**, S. H. Hosseinian***, and A. Jalilian****

Abstract: Nowadays study of input voltage quality on induction motors behavior has become a controversial subject due to the wide application of these motors in the industry. The impact of grid voltage fluctuations on the performance of induction motors can be included in this area. The majority of papers devoted to the influence of voltage fluctuations on the induction motors are focusing only on the solving of d-q state equations or steady-state equivalent circuit analysis. In this paper, a new approach to this issue is investigated by field analysis which studies the effects of voltage fluctuations on the magnetic fluxes of induction motors. New analytical expressions to approximate the airgap flux density and the torque under-voltage fluctuation conditions are presented. These characteristics are also calculated directly by the finite-element method considering the magnetic saturation and the harmonic fields. Finally, experimental results on a typical induction motor are employed to validate the accuracy of analytical and simulation results.

Keywords: Induction Motor, Finite Element Method, Field Study, Voltage Fluctuation.

Nomenclature

δ_g	Air gap length [m]
φ_r	Angular displacement of rotor [Deg.]
φ_s	Angular displacement of stator [Deg.]
ω_b	Angular frequency of the supply [rad/s]
ω_m	Angular modulation frequency [rad/s]
k_{c2}	Carter coefficient of rotor
k_{c1}	Carter coefficient of stator
T_e	Electromagnetic torque [N.m]
W_m	Energy stored in the magnetic field of the air gap [J]
f_b	Fundamental frequency [Hz]
V_p	Line to neutral peak voltage [V]
T_L	Load torque [N.m]
k_m	Modulation depth
f_m	Modulation frequency [Hz]
D	Motor diameter [m]
R	Number of rotor slot
N_1	Number of turns in the stator winding of one phase
B_r	Peak amplitude of fundamental component of rotor flux density [T]
B_s	Peak amplitude of fundamental component of stator flux density [T]
B_{rn}	Peak amplitude of the lower frequency component of rotor flux density [T]
B_{sn}	Peak amplitude of the lower frequency component of stator flux density [T]
B_{rp}	Peak amplitude of the upper frequency component of rotor flux density [T]
B_{sp}	Peak amplitude of the upper frequency component of stator flux density [T]
φ_0	Phase angle of the no-load current
φ_1	Phase angle of the stator phase current
p	Pole pair number
k_{wv}	Resultant winding factor for the vth harmonic
B_2	Rotor flux density [T]
θ_r	Rotor position [Deg.]

Iranian Journal of Electrical and Electronic Engineering, 2021.
Paper first received 29 September 2019, revised 18 March 2020, and accepted 10 April 2020.
* The author is with the Department of Electrical Engineering, Sirjan University of Technology, Sirjan, Iran.
E-mail: mghaseminejad@sirjantech.ac.ir.
** The author is with the Department of Electrical Engineering, Shahed University, Tehran, Iran.
E-mail: doroudi@shahed.ac.ir.
*** The author is with the Department of Electrical Engineering, Amirkabir University of Technology, Tehran, Iran.
E-mail: hosseinian@aut.ac.ir.
**** The author is with the Department of Electrical Engineering, University of Science and Technology, Tehran, Iran.
E-mail: jalilian@iust.ac.ir.
Corresponding Author: M. Ghaseminezhad.
https://doi.org/10.22068/IJEEE.17.1.1620

ω_r	Rotor speed [rad/s]
s	Slip
s_m	Slip for maximum torque
B_1	Stator flux density [T]
l	Stator length [m]
μ_0	Vacuum permeability

1 Introduction

SEVERAL recent studies in power engineering have been concerned with voltage fluctuations. This type of power quality events has many undesirable effects on domestic and industrial loads. The most significant influence of voltage fluctuations is in the light flicker, which can be noticed on lamps as undesired illumination intensity variations [1]. Flicker frequencies in the range of 0.05 to 35 Hz can cause perceptible flicker [2]. Voltage fluctuations are simply an amplitude modulation signal which is usually expressed as a percent of the total change in voltage with respect to the average voltage over a specified time interval. The voltage waveform exhibits variations in magnitude due to the intermittent operation of connected loads. The instantaneous line to neutral voltage can be expressed as [3]:

$$v_a(t) = V_p\left(1+\sum_{m=1} k_m \sin(2\pi f_m t)\right)\cos(2\pi f_b t) \quad (1)$$

In the balanced systems, the other two phases can be defined in the same manner except in that the phase angle of base components in those should be modified by -120 and -240, respectively.

Heavy loads such as arc furnaces whose power demands are rapidly variable and light loads such as copying machines that are intermittent in time can lead to voltage fluctuations [4]. In addition to lamps, voltage fluctuations can also influence other sensitive electrical equipment [5].

Induction motors are widely used in many industrial, commercial, and residential applications because of various techno-economic advantages [6, 7]. It is estimated that more than 50% of the world's electrical energy generated is consumed by electric machines (mainly by induction motors) [8]. Therefore, it is important to analyze the effects of any disturbance such as voltage fluctuations on the behavior of induction motors.

The effect of voltage fluctuations on currents, speed, torque, and efficiency of induction motors was studied in [9-19]. For example, additional symmetrical voltage components produced by voltage fluctuations, creating some torque ripples and unintended noise and vibrations in the structure of the motor. These vibrations may lead to a reduction in the life expectancy of the mechanical components such as bearings and the joints. In [17], an equivalent circuit is presented to investigate the effect of voltage fluctuations on induction motor behavior regardless of speed changes. Simulation results were presented for induction motors with specifications given in [20]. These motors have a moment of inertia larger than that of the practical motor of the same size. Therefore the amplitude of obtained speed fluctuation is small and the results of the equivalent circuit have a good agreement with the large-signal simulations. In [18], the voltage fluctuation impact on induction motors by an innovative equivalent circuit considering speed changes was investigated. Efficiency, as well as the rotor and stator losses in the steady-state mode of operation were obtained. In [19], a two-dimensional finite element method is utilized to address the effect of supply voltage fluctuations on the ohmic and core losses of induction motors.

A quick survey of the literature shows that in most cases, simulations based on the d-q frame model are applied to analyze induction motor behavior under-voltage fluctuation conditions. However, this paper offers a new point of view to this subject by an analytical method based on the field analysis. The analytical approach gives insight into the stator, rotor and airgap field distributions, slot and MMF space harmonics and torque components of induction motors under-voltage fluctuation conditions. New analytical expressions to approximate the airgap flux density and the torque of induction motor under-voltage fluctuation conditions are presented. The analytical expressions can be used for studies about vibration and life expectancy of the mechanical components. Finally, experimental and finite element method results are employed to verify the results of the analytical approach.

The presented work is organized in the following manner: In Section 2, an analytical approach is utilized to investigate the induction motor response to voltage fluctuations. The results are verified by finite-element simulation in Section 3. Finally, Sections 4 and 5 provide experimental results and the conclusion of the paper.

2 Field Analysis of Induction Motor Under Voltage Fluctuation Conditions

In this section, an analytical approach is first developed to obtain the stator, rotor and resultant airgap flux densities under-voltage fluctuation conditions. Then, the motor torque is calculated mathematically using these flux densities. The focus has been on the torque components and the rotor behavior subjected to these components. Finally, the analysis is verified by the finite element method.

2.1 Air Gap Flux Density Components Caused by Voltage fluctuations

To evaluate the effects of voltage fluctuations on the induction motor flux density distribution, Eq. (1) can be rewritten as follows (m = 1):

$$v(t)=V_p\left[1+k\sin(\omega_m t)\right]\cos(\omega_b t)=V_p\cos(\omega_b t)+\frac{kV_p}{2}\cos\left[(\omega_b+\omega_m)t-\frac{\pi}{2}\right]-\frac{kV_p}{2}\cos\left[(\omega_b-\omega_m)t-\frac{\pi}{2}\right] \quad (2)$$

The first term in (2) is the voltage fundamental component. The second and third terms are the variations in voltage fluctuations, superimposed to fundamental component with $f_b + f_m$ (upper component) and $f_b - f_m$ (lower component) frequencies.

Balanced 3-phase currents flowing in the stator windings establish a rotating MMF in the air gap with the speed determined by the frequency of stator currents and the number of poles. The complex expressions of the fundamental and the spatial MMF harmonics of the stator are:

$$F_s(\varphi_s,t)=\frac{3\sqrt{2}N_1k_wI_0}{p\pi}\exp\left(j(p\varphi_s-\omega_b t-\varphi_0)\right)+\frac{3\sqrt{2}N_1k_{w\upsilon}I_s}{p\pi\upsilon}\sum_{\upsilon}\exp\left(j(p\upsilon\varphi_s-\omega_b t-\varphi_1)\right) \quad (3)$$

where

$$\upsilon=6g\pm1, g=\pm1,\pm2,... \quad (4)$$

The stepped distribution of the stator MMF produces harmonic airgap fields of order υ. The angular displacement along the stator circumference is denoted by φ_s. Similarly, additional current components created by voltage fluctuations would make additional MMF components in the air gap. Eq. (5) describes the additional MMF generated by the alternating currents in the stator windings when regular fluctuations appear in the terminals of induction motors.

$$\begin{aligned}\Delta F_s(\varphi_s,t)&=\frac{3\sqrt{2}N_1k_w}{p\pi}\left[I_{0p}\exp\left(j\left(\varphi_s-(\omega_b+\omega_m)t-\varphi_0-\frac{\pi}{2}\right)\right)\right.\\&\left.-I_{0n}\exp\left(j\left(\varphi_s-(\omega_b-\omega_m)t-\varphi_0-\frac{\pi}{2}\right)\right)\right]\\&+\frac{3\sqrt{2}N_1k_{w\upsilon}}{p\pi\upsilon}\left[I_{sp}\sum_{\upsilon}\exp\left(j\left(p\upsilon\varphi_s-(\omega_b+\omega_m)t-\varphi_1-\frac{\pi}{2}\right)\right)\right.\\&\left.-I_{sn}\sum_{\upsilon}\exp\left(j\left(p\upsilon\varphi_s-(\omega_b-\omega_m)t-\varphi_1-\frac{\pi}{2}\right)\right)\right]\end{aligned} \quad (5)$$

According to [17], the I_{0p}, I_{0n}, I_{sp}, and I_{sn} can be obtained by the upper and lower equivalent circuits shown in Fig. 1. The stator flux-density is given by the product of the MMF-wave and the permeance-wave.

$$B_1(\varphi_s,t)=\left(F_s(\varphi_s,t)+\Delta F_s(\varphi_s,t)\right)\times G_m$$
$$G_m=G_{m0}+G_{m\upsilon} \quad (6)$$

The permeance wave can be expressed as a summation of an average value and slots harmonics permeances. The following points are considered:

a) The stator permeance is calculated separately from the permeance of the rotor.
b) Stator/Rotor is slotted while the other is smooth.
c) The magnetic permeance is taken into account by ignoring the saturation harmonics.
d) The space harmonics of MMF waves created by the time harmonics of rotor currents (residual MMF waves) are neglected.

The average permeance of the airgap constrained by a smooth and a slotted surface, G_{m0}, can be calculated using the Carter coefficients, referring to the stator and rotor separately:

$$G_{m0}=\frac{\mu_0}{k_{c1}k_{c2}\delta_g} \quad (7)$$

In the case of smooth-rotors, the complex Fourier series of the magnetic permeance due to stator slots is expressed as [21]:

$$G_{m\upsilon}=G_{m0}k_{c1}\sum_{g=1}^{\infty}-(-1)^g\frac{\sin\left[g\pi(k_{c1}-1)/k_{c1}\right]}{g\pi/k_{c1}}\times\exp(jgS\varphi_s) \quad (8)$$

The instantaneous value of the flux density wave is the real part of the complex wave. The radial air gap flux density is thus given by:

$$\begin{aligned}B_1(\varphi_s,t)=&\\&\frac{3\sqrt{2}N_1k_w\mu_0}{p\pi k_{c1}k_{c2}\delta_g}\left[I_0\cos(p\varphi_s-\omega_b t-\varphi_0)\right.\\&\quad+I_{0p}\sin\left(p\varphi_s-(\omega_b+\omega_m)t-\varphi_{0p}\right)\\&\quad\left.-I_{0n}\sin\left(p\varphi_s-(\omega_b-\omega_m)t-\varphi_{0n}\right)\right]\\&+\frac{3\sqrt{2}N_1k_{w\upsilon}\mu_0}{p\pi\upsilon k_{c1}k_{c2}\delta_g}\left[\sum_{\upsilon}I_s\cos(p\upsilon\varphi_s-\omega_b t-\varphi_1)\right.\\&\quad+\sum_{\upsilon}I_{sp}\sin\left(p\upsilon\varphi_s-(\omega_b+\omega_m)t-\varphi_{1p}\right)\\&\quad\left.-\sum_{\upsilon}I_{sn}\sin\left(p\upsilon\varphi_s-(\omega_b-\omega_m)t-\varphi_{1n}\right)\right]\\&+\frac{-(-1)^g3\sqrt{2}N_1k_w\mu_0(k_{c1}-1)k_{v_{sl}}}{p\pi\upsilon k_{c1}k_{c2}\delta_g}\times\\&\quad\left[\sum_{v_{sl}}I_s\cos(pv_{sl}\varphi_s-\omega_b t-\varphi_0)\right.\\&\quad+\sum_{v_{sl}}I_{sp}\sin\left(pv_{sl}\varphi_s-(\omega_b+\omega_m)t-\varphi_{0p}\right)\\&\quad\left.-\sum_{v_{sl}}I_{sn}\sin\left(pv_{sl}\varphi_s-(\omega_b-\omega_m)t-\varphi_{on}\right)\right]\end{aligned} \quad (9)$$

where

$$k_{v_{sl}}=\frac{\sin\left[g(k_{c1}-1)\pi/k_{c1}\right]}{\left[g(k_{c1}-1)\pi/k_{c1}\right]},\ v_{sl}=\frac{gS}{p}+1, g=\pm1,\pm2,... \quad (10)$$

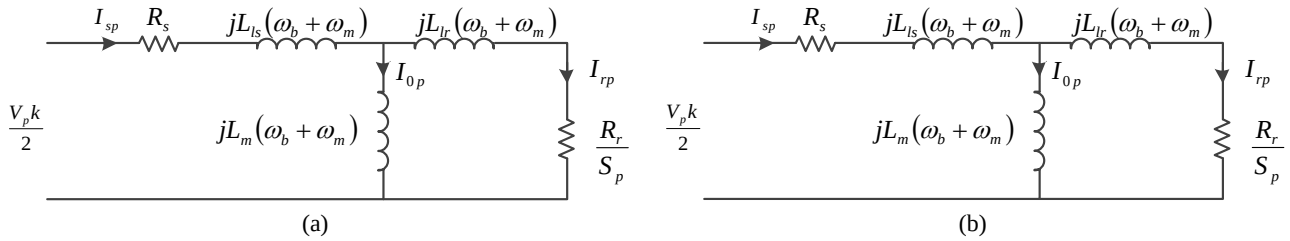

Fig. 1 Upper and lower frequencies equivalent circuits of induction motor under-voltage fluctuation conditions (V_p=V_n= Terminals Phase Voltage).

$$
\begin{aligned}
B_1(\varphi_s,t) = {} & \frac{3\sqrt{2}N_1 k_w \mu_0}{p\pi k_{c1}k_{c2}\delta_g}\Big[I_0\cos\phi_1\cos\big(p\varphi_r-(\omega_b-\omega_r)t-\psi_r\big)+I_{0p}\cos\phi_{1p}\sin\big(p\varphi_r-\big[(\omega_b+\omega_m)-\omega_r\big]t-\psi_r\big) \\
& -I_{0n}\cos\phi_{1n}\sin\big(p\varphi_r-\big[(\omega_b-\omega_m)-\omega_r\big]t-\psi_r\big)\Big] \\
& +\frac{3\sqrt{2}N_1 k_{w\lambda}\mu_0}{p\pi\lambda k_{c1}k_{c2}\delta_g}\Big[\sum_{\lambda}I_s\cos\phi_1\cos\big(p\lambda\varphi_r-(\omega_b-\omega_r)t-\psi_{r\lambda}\big) \\
& +\sum_{\lambda}I_{sp}\cos\phi_{1n}\sin\big(p\lambda\varphi_r-\big[(\omega_b+\omega_m)-\omega_r\big]t-\psi_{r\lambda}\big) \\
& -\sum_{\lambda}I_{sn}\cos\phi_{1p}\sin\big(p\lambda\varphi_r-\big[(\omega_b-\omega_m)-\omega_r\big]t-\psi_{r\lambda}\big)\Big] \\
& +\frac{-(-1)^g 3\sqrt{2}N_1 k_w \mu_0 (k_{c2}-1)k_{\lambda_{sl}}}{p\pi\lambda k_{c1}k_{c2}\delta_g}\Big[\sum_{k_{\lambda_{sl}}}I_s\cos\phi_1\cos\big(p\lambda_{sl}\varphi_r-(\omega_b-\omega_r)t-\varphi_0\big) \\
& +\sum_{k_{\lambda_{sl}}}I_{sp}\cos\phi_{1p}\sin\big(p\lambda_{sl}\varphi_r-\big[(\omega_b+\omega_m)-\omega_r\big]t-\varphi_0\big) \\
& -\sum_{k_{\lambda_{sl}}}I_{sn}\cos\phi_{1n}\sin\big(p\lambda_{sl}\varphi_r-\big[(\omega_b-\omega_m)-\omega_r\big]t-\varphi_0\big)\Big]
\end{aligned}
\tag{11}
$$

As shown in (9), Stator flux density has three obvious components:

a) Fundamental and its sideband components

b) Spatial MMF harmonics and their sideband components

c) Harmonics due to variations of permeance and their sideband components.

All sideband components are created due to voltage fluctuations. Since the stator and rotor windings are placed in the slots, the MMF-wave itself has its own harmonics. These harmonics are indistinguishable from those caused by variations of permeance due to slotting.

The Stator flux density wave components affect the rotor through the air gap and induce a voltage in the rotor windings. The induced voltages create circulating currents in the closed rotor circuits depend on the rotor windings impedance. This impedance is a function of frequency, the number of turns, the number of slots, the permeability of iron, and so forth [21]. The rotor currents develop MMF waves of their own. Rotor flux density can be obtained by the product of the MMF wave of the rotor and the airgap permeance wave as (11), where

$$k_{\lambda_{sl}} = \frac{\sin\big[g(k_{c2}-1)\pi/k_{c2}\big]}{\big[g(k_{c1}-1)\pi/k_{c1}\big]}$$

$$\lambda = \lambda_{sl} = \frac{gR}{p}+1, \qquad g=\pm1,\pm2,\ldots$$

$$\psi_r = \psi_{r\lambda} = \varphi_1 + \frac{I_0 s_m}{I_{sc} s} \tag{12}$$

The angular displacement along the rotor circumference is denoted by φ_r and θ_r is the angular displacement of the rotor. The relationships between φ_r, φ_s, and θ_r are given by:

$$\varphi_s = \varphi_r + \theta_r, \qquad \theta_r = \frac{(1-s)\omega_b t}{p} \tag{13}$$

Finally, the resultant air-gap flux density can be calculated from (9)-(13) by superposition of rotor and stator flux densities. Figure 2 shows the calculated airgap flux density and its normalized frequency spectrum for a given induction motor (The ratings and main parameters of the induction motor are listed in Table 1. As it is seen, in addition to the fundamental component, its sideband components (the lower and upper) are clearly shown in the figure. Furthermore, at 814, 914, 1680, and 1780 Hz, slot harmonics and their sideband components with significant amplitudes are obviously seen in the frequency spectrum. All results

are summarized in Table 2. According to the third term in (11), the principal slot harmonics of the air gap flux density can be expressed as:

$$Psh = \left(\frac{gR}{p}(1-s)+1 \right) f_b \tag{14}$$

The induction motor has R = 18 rotor slots and its rotor speed is n_r = 2880 rpm. Therefore, slot harmonics can be easily derived from (14).

2.2 The Motor Torque

Voltage fluctuations can create torque ripples. To explain it mathematically, the motor torque is calculated using the flux densities of rotor and stator obtained from the previous section. For simplicity, the fundamental component of the rotor and stator flux densities will be used and the slotting and space harmonics are ignored. The electromagnetic torque can be expressed as [21]:

$$T_e = \frac{\partial W_m}{\partial \theta_r} \tag{15}$$

where W_m is given by:

$$W_m = \frac{\pi D \delta_g l}{2\mu_0} \int_0^{2\pi} \left[B_1(\varphi_s, t) + B_2(\varphi_s, t) \right]^2 d\varphi_s \tag{16}$$

Since $B_1(\varphi_s, t)$ is independent of the rotor position, the electromagnetic torque can be rewritten as:

$$T_e = \frac{\pi D \delta_g l}{2\mu_0} \int_0^{2\pi} 2\left[B_1(\varphi_s, t) + B_2(\varphi_s, t) \right] \frac{\partial B_2}{d\theta_r} d\varphi_s \tag{17}$$

It is apparent that the second term vanishes since:

$$\int_0^{2\pi} \sin\alpha \cos\alpha d\alpha = 0 \tag{18}$$

By substituting (9) and (11) in (14), motor torque expression is calculated as:

Table 1 The motor parameters.

Description	Value	Description	Value
Specification			
Nominal power	1100 W	Nominal voltage	220 V
Frequency	50 Hz	Nominal speed	2825 rpm
Stator			
Number of stator slot	24	Core length	80 mm
Outer diameter	120 mm	Stacking factor	0.95
Inner diameter	62 mm	Connection type	Wye
Number of pole	2	Number of phase	3
Strands per conductor	1	Conductor per slot	70
Rotor			
Inner Diameter	24.5 mm	Endring width	10 mm
Outer diameter	61 mm	Endring height	10 mm
Number of rotor slot	18	Core length	80 mm
Material	Aluminum	Stacking factor	0.95

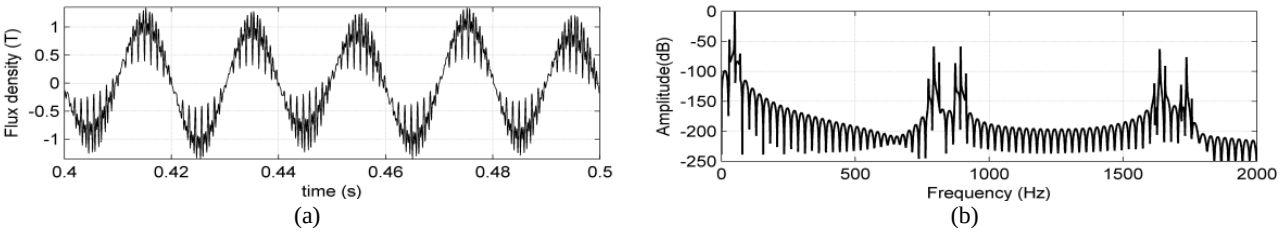

(a) (b)

Fig. 2 Air-gap flux density calculated by analytical approach under voltage fluctuation conditions (f_m = 20 Hz and k_m = 0.05).

Table 2 Calculated air-gap flux density components by analytical approach under-voltage fluctuation conditions (f_m = 20 Hz and k_m = 0.05).

Central frequency [Hz]	Amplitude [dB]	Sideband frequency [Hz]	Amplitude [dB]
50	0	30	-47.1
		70	-70.38
814	-58.8	794	-113.4
		834	-85.1
914	-58.8	894	-86.4
		934	-103.4
1680	-63.1	1660	-120.2
		1700	-90.8
1780	-76.4	1760	-122
		1800	-145.3

$$T_e = \frac{\pi^2 D \delta_g l}{\mu_0}\Big[B_s B_r \sin(-\psi_r) + B_s B_{rp} \sin(-\omega_m t - \psi_r) + B_s B_m \sin(\omega_m t - \psi_r) + B_{sp} B_r \sin(\omega_m t - \psi_r) + B_{sp} B_{rp} \sin(-\psi_r) + B_{sp} B_m \sin(2\omega_m t - \psi_r) + B_{sn} B_r \sin(-\omega_m t - \psi_r) + B_{sn} B_{rp} \sin(-2\omega_m t - \psi_r) + B_{sn} B_m \sin(-\psi_r)\Big] \quad (19)$$

As shown in (18), the average torque produced by the induction motor when subjected to fluctuated voltages consists of three different components; The first component is related to the interaction of the fundamental components of stator and rotor MMF $B_sB_r\sin(-\psi_r)$, The second one is based on the joint action of the upper components of stator and rotor MMF $B_{sp}B_{rp}\sin(-\psi_r)$, and the last one is the interaction of the lower components of stator and rotor MMF $B_{sn}B_{rn}\sin(-\psi_r)$. For an average torque to be produced, the magnetic field components of the stator and rotor must be stationary with respect to each other. Since the relative motion of the upper component of the stator field and the lower component of the rotor field is not zero, the interaction of these components produces no average torque. Joint actions of the upper and lower components of the stator and rotor MMF yields a pulsating torque component with the frequency of twice of modulation frequency. The latter case has relatively negligible magnitude (so can be easily ignored), because in principal the multiplication of upper and lower flux density components is very small. The terms obtained from the interaction of the main component and upper/ lower flux density components have a significant amplitude and pulsate at the modulation frequency (ω_m). Consequently, the electromagnetic torque of induction motor has an average value and a term with significant amplitude which pulsates at the modulation frequency as expressed in the following equation:

$$T_e = \frac{\pi^2 D \delta_g l}{\mu_0}\Big[T_{avg} + (B_s B_{rp} + B_{sn} B_r)\sin(-\omega_m t - \psi_r) + (B_s B_m + B_{sp} B_r)\sin(\omega_m t - \psi_r)\Big] \quad (20)$$

$$T_{avg} = B_s B_r \sin(-\psi_r) + B_{sp} B_{rp} \sin(-\psi_r) + B_{sn} B_{rn} \sin(-\psi_r)$$

Assuming a constant load torque, the dynamic motion (Eq. (21)) shows that the torque pulsations obtained in (19) cause speed fluctuations of the same frequency.

$$T_e = J\left(\frac{1}{p}\right)\frac{d\omega_r}{dt} + T_L \quad (21)$$

Fig. 3 shows the calculated motor torque at rated load, based on (19), under-voltage fluctuation conditions with modulation depth of 5% and modulation frequency of 20 Hz. Torque fluctuations with frequency of 20 Hz are obvious in Fig. 3. The peak to peak value of torque is also about 2.2 N.m (about 59% rated values).

3 Verification by Finite Element Method

The finite element method (FEM) rapidly grew as the most useful numerical analysis tool to study and design of electric machines. The finite element method with the addition of time-stepping can provide a quite accurate prediction of transient performance of electrical machines [15]. The advantage of this technique is that magnetic saturation and space distribution of stator and rotor windings can be taken into account.

The design parameters of the motor (listed in Table 1) are applied in FE analysis. This motor has a one-layer lap stator winding, arranged for three phases and two poles in 24 stator slots. The rotor is an aluminum cage with 18 slots.

The rotor slots are not skewed. The stator and rotor cores are made of steel sheet laminations with 3.5% silicon and 0.5 mm thickness.

The nonlinear characteristic of the core materials has been taken into account in the finite element analysis. Three balanced fluctuated voltages are applied to the motor terminals by the use of external circuits. The flux

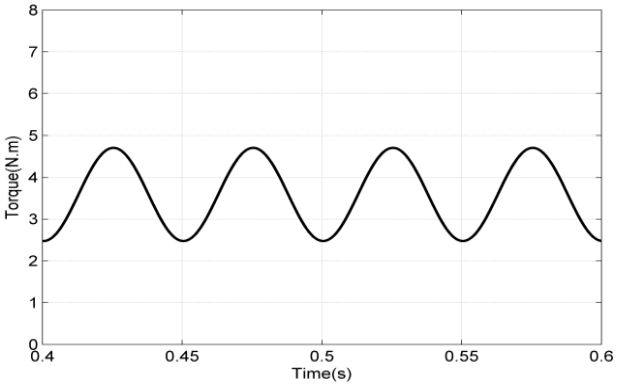

Fig. 3 Calculated torque by analytical approach under voltage fluctuations (f_m = 20 Hz and k_m = 0.05).

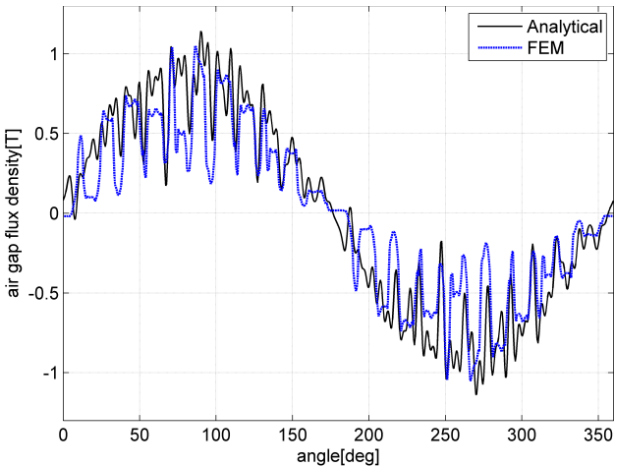

Fig. 4 Air-gap flux density distribution under-voltage fluctuation conditions obtained from FEM and analytical approach (f_m = 20 Hz and k_m= 0.05).

density distribution obtained from FEM simulation under-voltage fluctuation conditions is shown in Fig. 4. For comparison, the analytical results have been also shown in this figure. A good agreement can be seen between the FEM and the analytical results. The variations of flux density versus time and its frequency spectrum at one point in the middle of airgap lying directly under a stator tooth (hereafter called point A) in two cases; normal operation and under-voltage fluctuation conditions have been illustrated in Fig. 5. Similar to the analytical approach, the slot harmonics can be indicated by arrows in 814, 914, 1680, and 1780 Hz.

Comparing the results of FEM and the analytical approach shows more frequency components around the slot harmonics in the FEM results. The reason for this is the fact that space harmonic MMF waves created by the time harmonics of the currents in the rotor windings and their effects are not considered in the analytical approach (assumption "d" in section 2.1).

Variations of motor torque and speed for a 20 Hz modulation frequency determined by FEM simulation are shown in Fig. 6. It is clear that the speed and torque of the motor pulsate at the modulation frequency as knowledge gained by the analytical approach. However, there are some ripples in torque in Fig. 6 which do not observe in the analytical approach. This happens because of the fact that in the analytical approach, torque calculations were done by ignoring the total slot and space harmonics.

The stator current, voltage and flux linkage of phase A and their frequency spectrums under-voltage fluctuation conditions are illustrated in Fig. 7. As it is seen, the same fundamental voltage magnitude of upper and lower components establishes different magnitudes of current at corresponding frequencies. Referring to the equivalent circuits shown in Fig. 1, this occurs due to smaller effective input impedance of the motor at the lower frequency (30 Hz) compared with the upper frequency (70 Hz). Also, relatively negligible current components at frequencies of $f_b \pm 2jf_m$ (j = 1, 2, 3, …) are seen in the figure.

4 Experimental Results

In this section, the numerical results are validated under laboratory conditions. A 61704-Chroma programmable AC source supplies 1.1 kW induction

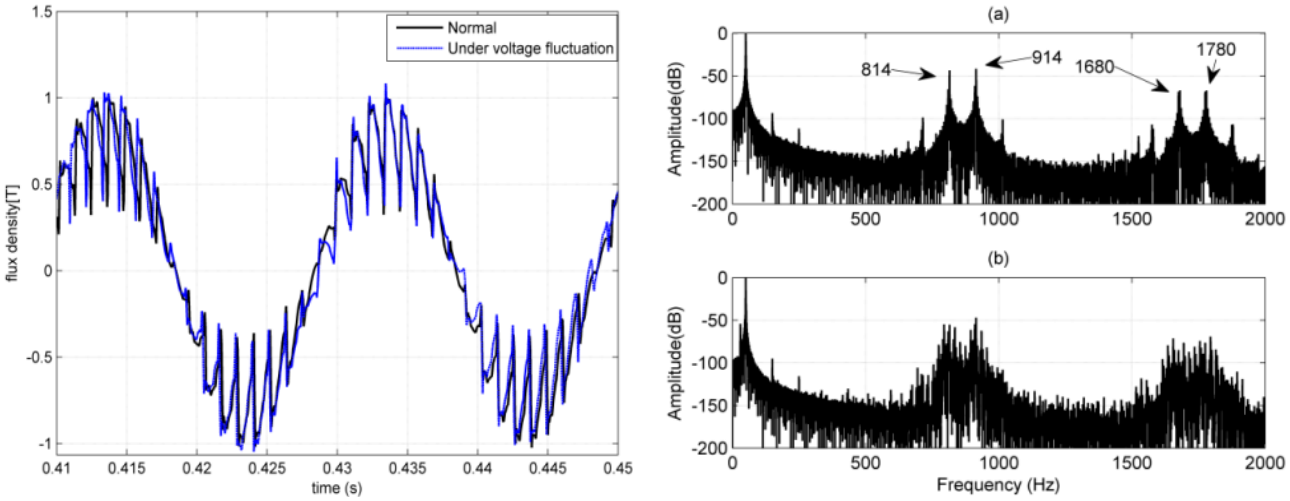

Fig. 5 Magnetic flux density curves (left) and their frequency spectrum (right) at point A in two cases; a) normal b) under fluctuated voltages (f_m= 20 Hz and k_m = 0.05).

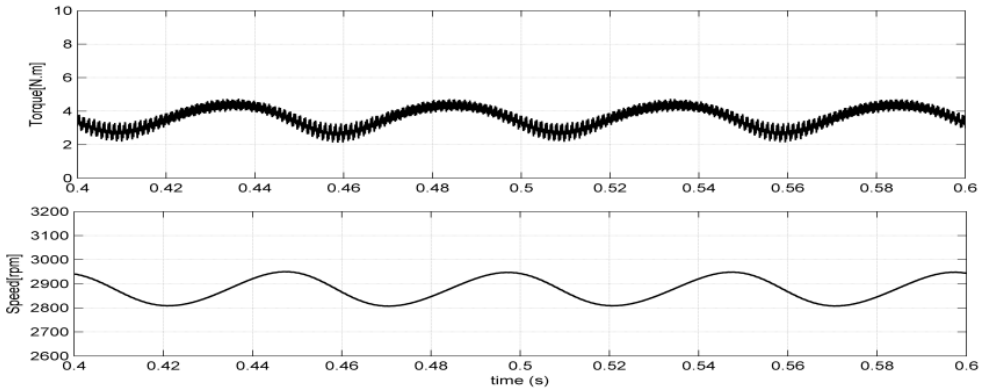

Fig. 6 Motor speed and torque variations under-voltage fluctuation conditions obtained by FEM (f_m= 20 Hz and k_m= 0.05).

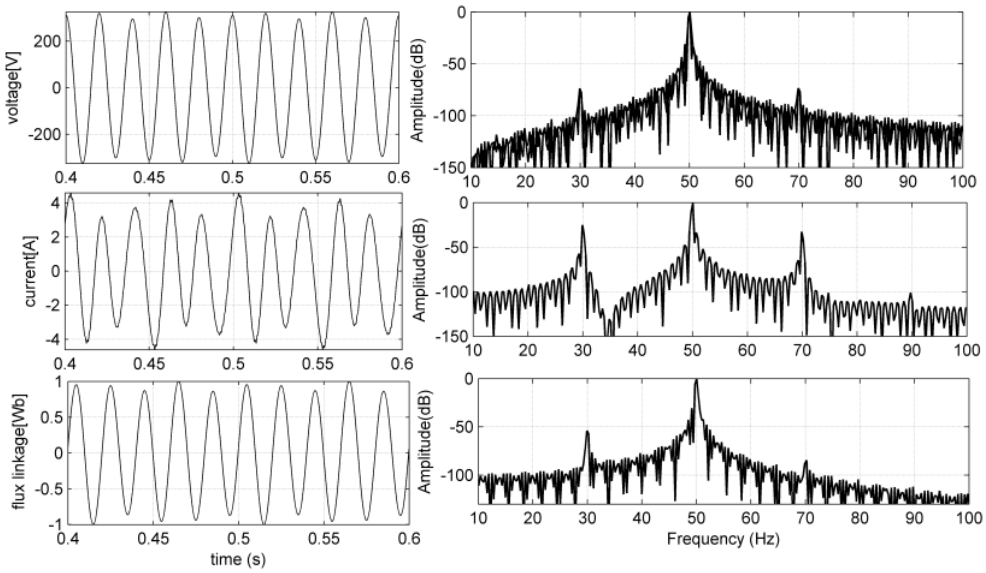

Fig. 7 Frequency spectrum of current, voltage, and flux linkage under fluctuated conditions obtained by FEM (f_m= 20 Hz and k_m = 0.05).

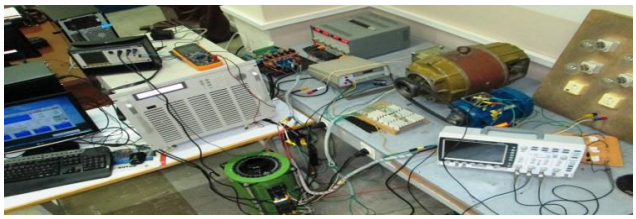

Fig. 8 Overview of the complete experimental setup.

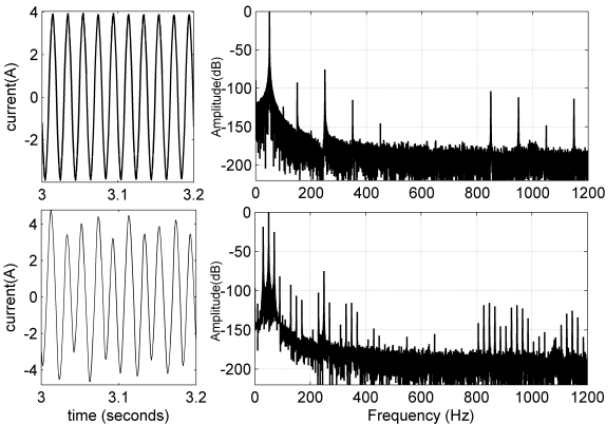

Fig. 9 Measured current under normal and voltage fluctuation conditions (f_m = 20 Hz and k_m = 0.05).

motor. To vary the load conditions, a 1.5 kW DC generator is coupled by a belt and pulley to the tested motor. An encoder is fastened to the shaft of the motor as an angular speed sensor to measure and records the speed changes versus time. LEM-LA-100-P and 5CSNE151 Honeywell current transducer sensors are used in the data conditioning board. PCI-1710HG Advantech DAQ card acquires and transfers all data to a PC. Fig. 8 shows an overview of the complete experimental setup.

The waveforms captured in Fig. 9, show the measured stator current and their frequency spectrums under normal (top) and voltage fluctuation conditions (bottom). The slot and saturation harmonics can be clearly seen in both normalized frequency spectrums while the upper and lower frequency components around each harmonic are only observed under-voltage fluctuation conditions. Some additional harmonics can also be seen in the frequency spectrum under-voltage fluctuation conditions. According to [18], variations of speed due to the voltage fluctuations result in the appearance of these additional components.

To measure the airgap flux density, a search coil with integral pitch is located in the air gap and in the middle of a slot opening. The airgap flux density is measured using the induced voltage in this coil. Induced voltage has the same waveform as the resulting air gap flux density and the relationship is:

$$E_j = 2lvB_j = 2l\frac{\pi D n_r}{60}\frac{B_{jm}}{\sqrt{2}} \tag{22}$$

Fig. 10 shows the air gap flux density. For comparison, the airgap flux obtained from the analytical approach is also given in the figure. Table 3 compares FEM, analytical and experimental results. There is a good agreement between the simulations and experimental results.

Finally, the experimental waveforms of the motor speed is given in Fig. 11 and compared with the speed

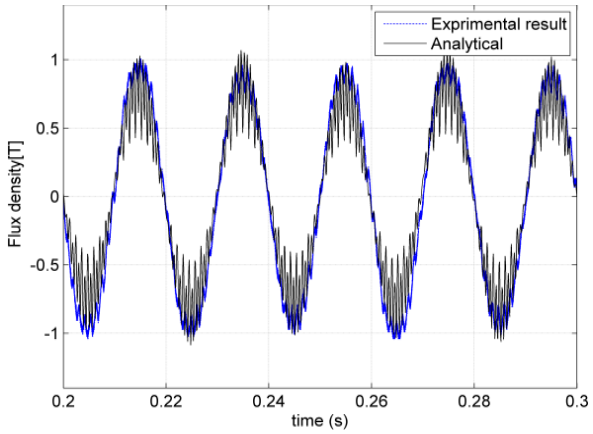

Fig. 10 Airgap flux density under-voltage fluctuation conditions (f_m=20 Hz and k_m = 0.05).

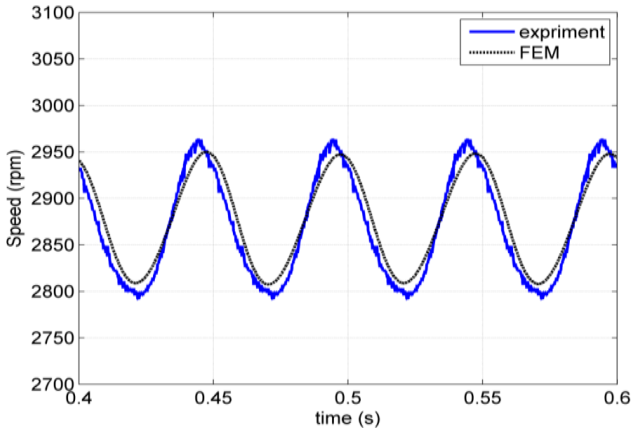

Fig. 11 Measured and FEM speed fluctuations under voltage fluctuation conditions (f_m = 20 Hz and k_m = 0.05).

Table 3 comparison of air-gap flux density components under voltage fluctuation conditions (f_m = 20 Hz and k_m = 0.05).

	Amplitude [T]		
Frequency [Hz]	Analytical	FEM	Experimental
50	0.8958	0.8035	0.8081
30	0.0884	0.06817	0.07817
70	0.02819	0.01844	0.02235

fluctuations obtained by FEM. A good correlation can be seen between the FEM and experimental results.

5 Conclusion

In this paper, electromagnetic field components of both the stator and rotor have been analytically evaluated to show resultant airgap and torque components. How motor torque pulsates with modulation frequency can be proved by the proposed analytical approach. The proposed analytical method can be also calculated as new electromagnetic field components under-voltage fluctuation conditions. Finite element analysis was employed to obtain the flux distribution and the other motor quantities. The FEM and experimental results show good agreement with the results of the analytical approach. These analytical expressions can be used for optimization problems and studies about vibration and life expectancy of the mechanical components.

References

[1] M. Rahimi and H. Assari, "Addressing and assessing the issues related to connection of the wind turbine generators to the distribution grid," *International Journal of Electrical Power and Energy Systems*, Vol. 86, pp. 138–153, 2017.

[2] H. Moghadam Banayem, A. Doroudi, and M. Poormonfared Azimi, "Flicker source tracing by wavelet transform," *Electric Power Components and Systems*, Vol. 43, No. 4, pp. 412–421, 2015.

[3] J. Arrillaga, N. R. Watson, and S. Chen, *Power system quality assessment*. John Wiley & Sons Chichester, England, 2000.

[4] A. N. Gogdare, A. Doroudi, and M. Ghaseminejad, "A new method to mitigate voltage fluctuation of a fixed speed wind farm using DFIG wind turbine," in *Proceedings of 17th Conference on Electrical Power Distribution*, pp. 1–6, 2012.

[5] K. Zhao, P. Ciufo, and S. Perera, "Induction motors subject to regular voltage fluctuations: Stator and rotor current analysis from a heating perspective," in *IEEE 15th International Conference on Harmonics and Quality of Power*, pp. 642–648, 2012.

[6] M. B. K. Bouzid, G. Champenois, and S. Tnani, "Reliable stator fault detection based on the induction motor negative sequence current compensation," *International Journal of Electrical Power & Energy Systems*, Vol. 95, pp. 490–498, 2018.

[7] A. Sapena-Bano, J. Martinez-Roman, R. Puche-Panadero, M. Pineda-Sanchez, J. Perez-Cruz, and M. Riera-Guasp, "Induction machine model with space harmonics for fault diagnosis based on the convolution theorem," *International Journal of Electrical Power & Energy Systems*, Vol. 100, pp. 463–481, 2018.

[8] K. Komeza and M. Dems, "Finite-element and analytical calculations of no-load core losses in energy-saving induction motors," IEEE Transactions on Industrial Electronics, Vol. 59, No. 7, pp. 2934–2946, 2012.

[9] M. GhasemiNezhad, A. Doroudi, and S. Hosseinian, "Evaluation of the effects of the regular voltage fluctuations on induction motors behavior," in *24th international Power System Conference*, Tehran, 2009.

[10] P. Gnaciński and M. Pepliński, "Induction cage machine supplied with voltage containing subharmonics and interharmonics," *IET Electric Power Applications*, Vol. 8, No. 8, pp. 287–295, 2014.

[11] M. Ghaseminezhad, A. Doroudi, and S. H. Hosseinian, "Double-cage induction motors behavior under flicker conditions," *Journal of Electric Power & Energy Conversion Systems*, Vol. 1, No. 1, pp. 1–7, 2016.

[12] M. Ghaseminezhad, A. Doroudi, S. H. Hosseinian, and A. Jalilian, "An investigation of induction motor saturation under voltage fluctuation conditions," *Journal of Magnetics*, Vol. 22, No. 2, pp. 306–314, 2017.

[13] P. Gnaciński, M. Pepliński, and D. Hallmann, "Cage induction machine under voltage subharmonics combined with voltage deviation," in *XIII International Conference on Electrical Machines (ICEM)*, pp. 1095–1100, 2018.

[14] P. Gnaciński and M. Pepliński, "Load-carrying capacity of induction machine supplied with voltage containing subharmonics," in *19th European Conference on Power Electronics and Applications (EPE'17 ECCE Europe)*, pp. 1–6, 2017.

[15] P. Gnaciński, D. Hallmann, M. Pepliński, and P. Jankowski, "The effects of voltage subharmonics on cage induction machine," *International Journal of Electrical Power & Energy Systems*, Vol. 111, pp. 125–131, 2019.

[16] P. Gnacinski, M. Pepliński, D. Hallmann, and P. Jankowski, "Induction cage machine thermal transients under lowered voltage quality," *IET Electric Power Applications*, Vol. 13, No. 4, pp. 479–476, 2019.

[17] M. Ghaseminezhad, A. Doroudi, and S. Hosseinian, "A novel equivalent circuit for induction motors under voltage fluctuation conditions," *AUT Journal of Electrical Engineering*, Vol. 44, No. 1, pp. 53–61, 2012.

[18] M. Ghaseminezhad, A. Doroudi, S. H. Hosseinian, and A. Jalilian, "Analysis of voltage fluctuation impact on induction motors by an innovative equivalent circuit considering the speed changes," *IET Generation, Transmission & Distribution*, Vol. 11, No. 2, pp. 512–519, 2017.

[19] M. Ghaseminezhad, A. Doroudi, S. H. Hosseinian, and A. Jalilian, "Investigation of increased ohmic and core losses in induction motors under voltage fluctuation conditions," *Iranian Journal of Science Technology, Transactions of Electrical Engineering*, Vol. 43, No. 2, pp. 373–382, 2019.

[20] P. C. Krause, O. Wasynczuk, S. D. Sudhoff, and S. Pekarek, *Analysis of electric machinery and drive systems*. Wiley Online Library, 2002.

[21] H. A. Toliyat and G. B. Kliman, *Handbook of electric motors*. CRC Press, 2004.

M. Ghaseminezhad was born in Bardsir, Iran, in 1985. He received the B.Sc. degree from the Electrical Engineering Department of Shahid Bahonar University, Kerman, Iran, in 2007 and the M.Sc. and Ph.D. degrees in Electrical Engineering from Shahed University, Tehran, Iran, in 2010, and 2017, respectively. At the present, he is an Assistant Professor of Electrical Engineering department at Sirjan University of Technology. His special fields of interest include transient in power systems, power quality, and electrical machines.

A. Doroudi was born in 1968 in Tehran, Iran. He received the B.Sc. degree from the Electrical Engineering Department of Amirkabir University of Technology, Tehran, Iran, in 1992 and the M.Sc. degree in Electrical Engineering from Tabriz University, Tabriz, Iran, in 1994 and the Ph.D. degree in Electrical Engineering from Amirkabir University of Technology, Tehran, Iran, in 2000. At the present, he is an Associate Professor of Electrical Engineering Department at Shahed University, Tehran, Iran. His special fields of interest include power quality, electric machines design, and power systems dynamic.

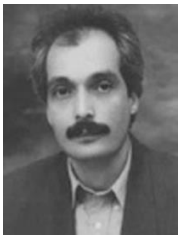

S. H. Hosseinian was born in 1961 in Iran. He received both the B.Sc. and M.Sc. degrees from the Electrical Engineering from Amirkabir University of Technology, Iran, in 1985, and 1988, respectively, and the Ph.D. degree in Electrical Engineering from the University of Newcastle England, 1996. At the present, he is a Professor of the Electrical Engineering Department at Amirkabir University of Technology (AUT). His special fields of interest include transient in power systems, power quality, restructuring and deregulation in power systems. he is the author of four books in the field of power systems. He is also the author and the co-author of over one hundred technical papers.

A. Jalilian was born in Yazd, Iran, in 1961. He received the B.Sc. degree in Electrical Engineering from Mazandaran University, Babol, Iran, in 1989, and the M.Sc. and Ph.D. degrees from the University of Wollongong, Wollongong, New South Wales, Australia, in 1992 and 1997, respectively. He joined the Power Group of the Department of Electrical Engineering at the Iran University of Science and Technology in 1998, where he is an Associate Professor. His research interests are causes, effects and mitigation of power quality problems in electrical systems and microgrids.